Imaging and measurement of cell structure and organization with submicron accuracy using light scattering spectroscopy

Vadim Backman[*1], Rajan Gurjar[2], Lev T. Perelman[3], Venkatesh Gopal[2], Maxim Kalashnikov[2], Kamran Badizadegan[4], Adam Wax[2], Irene Georgakoudi[2], Markus Mueller[2], Charles W Boone[2], Irving Itzkan[1], Ramachandra R. Dasari[2], and Michael S. Feld[**2]

[1]Biomedical Engineering Department, Northwestern University; [2]G. R. Harrison Spectroscopy Laboratory, Massachusetts Institute of Technology; [3]Harvard Medical School; [4]Department of Pathology, Children's Hospital, Harvard Medical School

ABSTRACT

Light scattering spectroscopy (LSS) is a promising optical technique developed for quantitative characterization of tissue morphology as well as *in vivo* detection and diagnosis of disease such as early cancer. LSS employs a wavelength dependent component of light scattered by epithelial cells and other tissues to obtain information about subcellular structure. We present two novel modalities of LSS, LSS imaging and scattering angle sensitive LSS (a/LSS). LSS imaging provides quantitative information about the epithelial cell nuclei, such as nuclear size, degree of pleomorphism, hyperchromasia, and amount of chromatin. It allows mapping these histological properties over wide areas of epithelial lining. We show that LSS imaging can be used to detect precancerous lesions in optically accessible organs. Using a/LSS, which enables characterization of tissue components with sizes smaller than the wavelength of light, we show that the number of subcellular components with the sizes between 30 nm and few microns scales with the size according to an inverse power-law. We show that the size distribution exponent is an important parameter characterizing tissue organization, for example the balance between stochasticity and order, and has a potential to be applicable for early cancer diagnosis and characterization.

Keywords: elastic scattering, polarization, dysplasia, cancer, nuclear atypia, cytology, fractal

1. INTRODUCTION

Light scattering spectroscopy (LSS) is extensively used in physical sciences to study a great variety of systems. Biological tissue can also be studied with LSS. Mourant *et al.*[1] and Perelman *et al.*[2] demonstrated that light scattering can provide structural and functional information about the tissue. Examining the structure of biological cells is an essential part of many clinical and laboratory studies. Histopathology, one of the most widely used methods of clinical diagnosis of disease, relies on assessing abnormal structure of cells by using a light microscope to study fixed and stained cells either from cell cultures or sectioned tissue samples obtained via biopsy. However, this useful and widely applied method has its limitations. Studies based on analysis of histological samples must contend with the artifacts which arise due to preparation. In addition, such analysis can only glimpse a snapshot in the life of an individual cell, instead relying on the study of large ensembles of cells to develop a picture of their time evolution.

Light scattering techniques offer an alternative to these approaches for studying the structure of live cells *in situ* by providing a non-invasive means of measuring cellular structure. In addition, since light scattering does not perturb the structure or function of cells, techniques based on light scattering permit studies of the development, formation and function of cellular structures through examination of the properties of the same cells at extended intervals. Elastically scattered light has been employed previously to probe the bulk properties of cells. For example, experiments using

[*] v-backman@northwestern.edu; Tel: (847) 491-3536; Fax: (847) 491-4918; Biomedical Engineering Department, Northwestern University, 2145 Sheridan Road, Evanston IL 60208, USA;
[**] msfeld@mit.edu; Tel: (617) 253-7700; Fax: (617) 258-6586; Room 6-014, Massachusetts Institute of Technology, 77 Massachusetts Ave., Cambridge, MA 02139, USA

goniometric[3,4] and fiber optic instruments[5] have helped develop models of light propagation based on Mie theory[6] and other methods.[7]

In LSS, white light is incident on the target particle, and its size and structure is determined from the wavelength dependence of the scattered light. Thus, elastic light scattering can be used to probe the morphology of live tissue. One complication of application of this approach is that in general, single scattering events cannot be directly measured in biological tissue.[8] Only a small portion of the light incident on the tissue is returned after a single scattering. The rest enters the tissue and undergoes multiple scattering from a variety of constituents in the underlying tissue, where it becomes randomized in direction, producing a large background of diffusely scattered light, the "diffusive background". The single scattering component must be distinguished from this background. This requires special techniques, because the diffusive background itself exhibits prominent spectral features dominated by the characteristic absorption bands of hemoglobin and scattering of collagen fibers, which are in abundance in the connective tissue beneath the epithelium. LSS aims to distinguish the single scattering component and analyze its spectral and angular properties in order to provide quantitative information about the morphology of the tissue. For example, as discussed below, LSS enables the measurement of the size and refractive index distribution of epithelial cell nuclei and, thus, quantitative characterization of the nuclear enlargement, crowding, hyperchromasia, and pleomorphism frequently associated with precancerous or cancerous transformations in virtually all types of epithelia.[9]

The basic principle underlying LSS is illustrated in Figure 1. Tissue under study is illuminated by visible light. LSS usually employs cw light to illuminate the tissue. However, illumination by narrowband light at a number of selected wavelengths can be used as well. The light, which is returned from the tissue by means of elastic scattering, is collected and its spectral and/or angular distribution is measured. This signal consists of two principal components: a single scattering component and multiple-scattering component. The multiple-scattering component is usually referred to as the "diffusive background". This terminology, although convenient, does not convey the full complexity of the process, because, generally, the multiply scattered light is not necessarily truly diffused. To isolate the single scattering component, the diffusive background is removed. There are two principal methods of diffusive background removal: (1) by mathematical modeling[2], and (2) using polarized light[10]. In the former case, a model, which uses absorption and scattering coefficients of the tissue as parameters to fit the spectral data, is applied to account for the diffusive background. The model fit is then subtracted leaving the single scattering component. The latter case uses the fact that the polarization of light is lost after multiple scattering events. By using linearly polarized incident light, the contribution due to single scattering can be obtained as the difference between the components of light scattered from the tissue polarized parallel and perpendicular to the direction of polarization of the incident light.

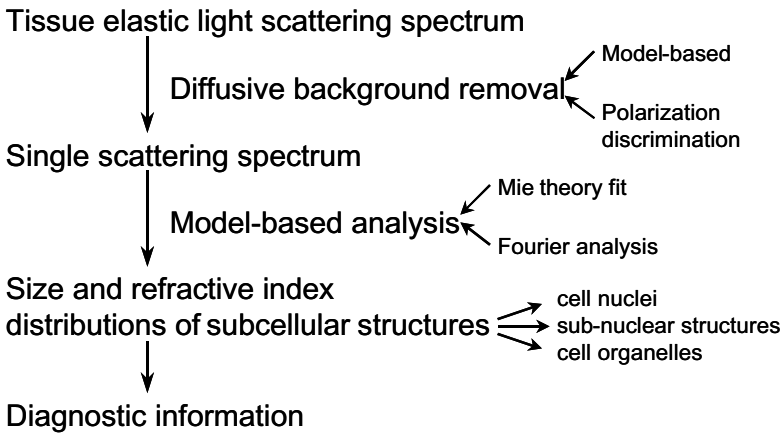

Figure 1. Principles of light scattering spectroscopy.

As long as the spectrum of the single scattering component is identified, it can be analyzed to obtain information about the properties of the scatterers responsible for this component. The origin of LSS signals depends on the geometry of light collection. For example, when light scattered in the near-backward directions is collected, the largest intracellular structures, the cell nuclei, are primarily responsible for the LSS signal. On the other hand, other collection geometries favor photons scattered by smaller sub-cellular structures with sizes comparable to or smaller than the wavelength of light. In any case, the spectrum of light scattered by these particles contains a component that varies characteristically with wavelength. This variation depends on particle size and refractive index. When particles of several sizes are present, the resulting signal is a superposition of these variations. Thus, the size distribution and refractive index of the scatterers can be determined from the analysis of the spectrum of light backscattered by these particles. Once the size distribution and refractive index are known, quantitative measures characterizing alterations of morphology of the epithelial cells can be obtained and corresponding diagnostic algorithms can be developed. For

example, if backscattering is observed, LSS enables the measurement of the size distribution of cell nuclei and their refractive index[2,10,11]. Thus, some of the major features characterizing nuclear atypia associated with precancerous and cancerous transformations, namely nuclear enlargement, crowding, and hyperchromasia, can be quantified. When light scattering with smaller scattering angles (larger backscattering angles) is collected, LSS signals are much less sensitive to the such large particles as cell nuclei and are primarily contributed by submicron cell constituents, such as intranuclear components, i.e. clumps of chromatin, and cytoplasmic organelles and inclusions, i.e. mitochondria, etc.[12]. Thus other cell features associated with precancerous transformations, such as abnormal chromatin texture, abnormal mitochondria, etc., can potentially be assessed.

2. PARAMETRIC LSS IMAGING

As mentioned above, LSS signals measured near the backscattering direction can provide information about the sizes and refractive indexes of the cell nuclei. LSS imaging technique has been developed that can map variations in the size of epithelial cell nuclei of living tissues over wide surface areas[13]. The resulting functional images provide direct quantitative measures of nuclear enlargement and chromatin content, which can be translated into clinical diagnoses. The technique can be used for non-invasive or minimally invasive detection of precancerous changes in a variety of organs, such as the colon and oral cavity.

Figure 2 shows the set-up for LSS imaging. A 75 W xenon arc lamp illuminates the sample which can be a living tissue, a cell monolayer or a physical tissue model. The light from the lamp is collimated, polarized and transmitted through one of 11 narrow-band (4 nm) filters to select the desired wavelength, λ_i i=1,…,11, in the range from 450 to 700 nm. This beam is delivered to the sample surface and illuminates an area of ~5 cm^2. A pair of equifocal achromatic lenses separated by twice their focal length collects the light backscattered from the sample. An aperture positioned at the center of the lens system ensures that the CCD detector (Princeton Instruments, Inc.), placed one focal length away from the outer lens, collects only light scattered in a solid angle corresponding to a half angle of 0.5°. This small angle of collection ensures that the major contribution to the signal is due to light scattered by the largest structures inside the cells, cell nuclei. This scheme allows 1:1 imaging of the illuminated surface. The CCD detector consists of a 512 x 512 pixel array, with each pixel having dimensions 25 μm x 25 μm. The analyzer is rotated to select the polarization state of the backscattered light.

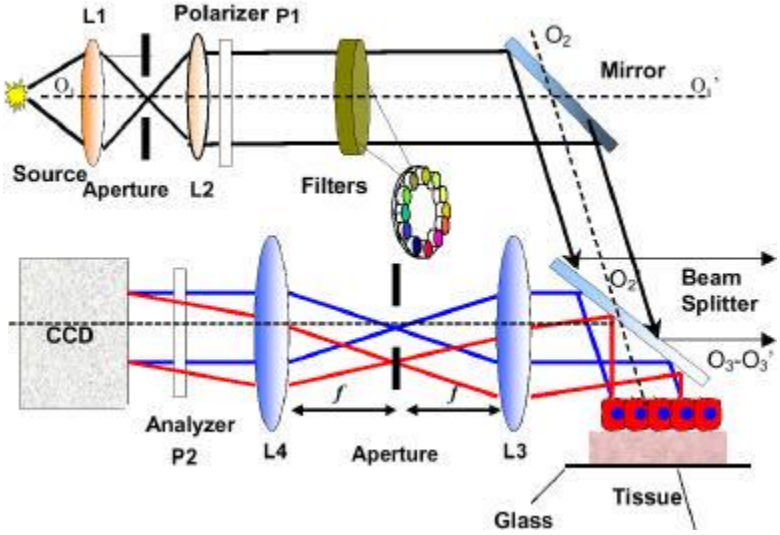

Figure 2. Schematic diagram of LSS imaging instrument.

The data acquisition is illustrated in Fig. 3. The CCD collects two images for each of the eleven illumination wavelengths. The first image, $I_{\parallel}(\lambda_i;x,y)$, with (x,y) pixel coordinates and wavelength λ_i, is taken with the analyzer oriented to collect backscattered light that is polarized along the polarization direction of the incident light. The second image, $I_{\perp}(\lambda_i;x,y)$, is taken with the analyzer oriented to collect the orthogonally polarized component. We then subtract $I_{\perp}(\lambda_i;x,y)$ from $I_{\parallel}(\lambda_i;x,y)$ to remove the contribution from the unpolarized diffusive background. This procedure results in an image $\Delta I(\lambda_i;x,y) = I_{\parallel}(\lambda_i;x,y) - I_{\perp}(\lambda_i;x,y)$ constituted almost entirely of single scattered photons, which, for most epithelial tissues, corresponds to a sampling depth of 30-50 μm.

The technique was first tested and the LSS imaging device was calibrated in a series of well-controlled experiments with physical tissue models. These experiments employed an optically thin layer of polystyrene beads (optical thickness τ=0.3) of several diameters, d = 4.5, 6 and 10 μm, with standard deviation of diameters $\sigma \approx 0.03$ μm, suspended in polyethylene glycol. The relative refractive index of the beads in glycol, 1.066, is in the range of relative refractive indices of biologically relevant structures, which typically vary between 1.02 and 1.10. In each case eleven

images $\Delta I(\lambda_i,x,y)$ were obtained for each of the wavelengths λ_i. The resulting spectra were in good agreement with the backscattered signals predicted by Mie theory. The spectra collected with the LSS imaging device were analyzed using the Mie theory-based inversion procedure[10]. The scatterers were assumed to be normally distributed in size. Mie theory was used to generate a data-base of LSS spectra over a range of mean diameters (from 0.1μm to 20μm in 0.005μm steps), standard deviations (from 0.1μm to 5μm in 0.005μm steps), and average relative refractive indexes (from 1.02 to 1.1 in 0.0005 steps). Then each of the spectra from this data-base was compared with the spectrum measured with LSS from any given pixel and the values of χ^2 were calculated. The sizes and refractive indexes of the scatterers that best fit the data were found. The wide range of sizes incorporated in the data-base ensured that the non-nuclear contribution to LSS signals was not ignored. Experiments with polystyrene beads of known size enabled us to estimate the accuracy of this inversion procedure. We found the size measurements to be accurate to 0.025 μm, and the refractive index measurements to be accurate to 0.001.

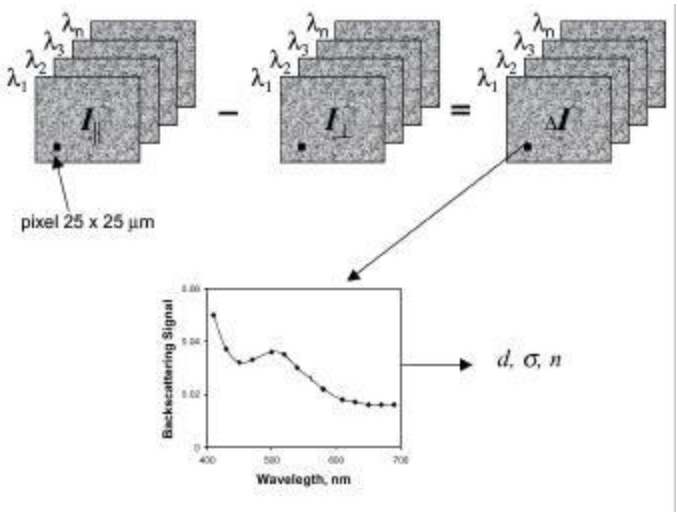

Figure 3. Schematic diagram illustrating the principles of data collection in LSS imaging.

The second series of experiments employed cells to model living tissue. The models consisted of two layers. The upper layer of the model simulated epithelium, and consisted of a monolayer of T84 colon tumor cells grown on a glass cover slip. The bottom layer was an optically thick solution of Ba_2SO_4 and hemoglobin simulating the connective tissue beneath the epithelium, which is primarily responsible for diffusing light. Before data collection, a portion of the cell layer was scraped off from the cover slip. The polarized images were then obtained. The imaged field was chosen so that the parts of the cover slip with and without cells were imaged. Figure 4 shows three images: (a) $I_{\|}(\lambda,x,y)$, (b) $I_{\perp}(\lambda,x,y)$, and (c) $\Delta I(\lambda,x,y)$, with λ=589 nm. Each image shows an area of 1.28 cm x 1.28 cm. Since cells are quite transparent, it was expected that most of the detected light (from 96% to 99% depending on wavelength) would originate from the second layer. However, this multiply scattered light is depolarized. In contrast, most of the light backscattered by the cells is polarized. Thus, although the cells are not discernable in either $I_{\|}(\lambda,x,y)$ or $\Delta I(\lambda,x,y)$ (Fig. 4(c)) as bright areas due to the signal of polarized light backscattered by these cells.

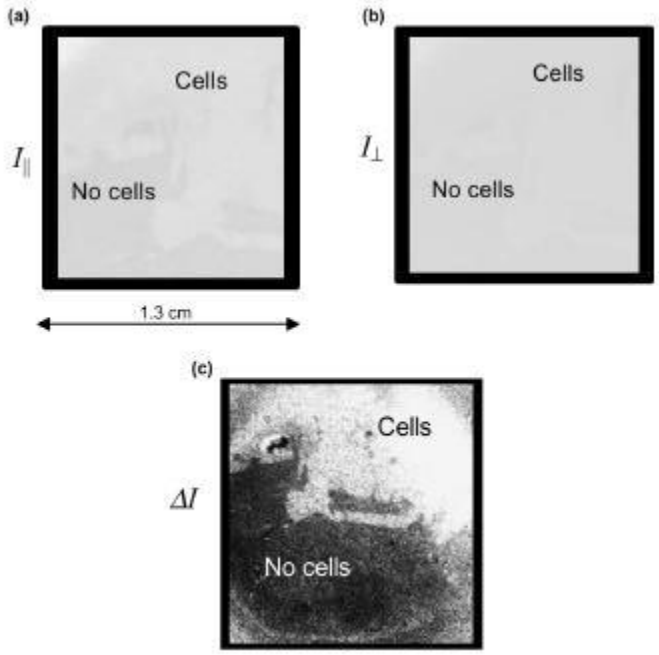

Figure 4. LSS imaging of a two-layer tissue model with a monolayer of T84 cells on top of a diffusive layer. Polarized backscattering signal is shown for λ=589 nm. (a) image $I_{\|}$; (b) image $I_{\perp}$; (c) image ΔI. Although the cells are not discernable on images (a) and (b), their backscattering is readily apparent when the diffusive background us removed using polarization discrimination on image (c).

An image collected for a single wavelength, such as one shown in Fig. 4(c), is not sufficient to obtain information about the sizes of the cell nuclei or other morphological properties of the cells. To obtain this information, a

succession of such images at different wavelengths must be taken, and the spectral curves $\Delta I(\lambda;x,y)$ must be analyzed for each pixel (x,y). Each pixel has 25 μm x 25 μm area and contains only few nuclei, typically 1 or 2. Some nuclei appear on two adjacent pixels, (x_1,y_1) and (x_2,y_2). Light backscattered by these nuclei contributes to both $\Delta I(\lambda;x_1,y_1)$ and $\Delta I(\lambda;x_2,y_2)$. To compensate for the cross-talk between neighboring pixels, we constructed new images for each wavelength λ, $\Delta I^{b}(\lambda,\bar{x},\bar{y})$ in which the intensity of any pixel is a weighted average of the values $\Delta I(\lambda;x,y)$ of the adjacent pixels from the original image,

$$\Delta I^{(b)}(\lambda;\bar{x},\bar{y}) = \sum_{i,j=-1,0,1} \Delta I(\lambda;x,y)a_{ij} \quad \text{with} \quad a = \begin{pmatrix} 0.075 & 0.125 & 0.075 \\ 0.125 & 0.2 & 0.125 \\ 0.075 & 0.125 & 0.075 \end{pmatrix}, \tag{1}$$

where the indexes $i,j = 0$ refer to the given pixel and $i,j = \pm 1$ to the adjacent pixels. This procedure is known to diminish the effect of the cross-talk[14].

T84 cells typically have a wide distribution of sizes and also have large mean diameters, d >10 μm. Figure 5 (a) shows a microphotograph of a portion of the cell monolayer stained with a nuclear stain that makes otherwise almost transparent cell nuclei appear blue. Color-coded contour plots of the cell nuclear sizes from a typical 275 μm x 125 μm region of the monolayer obtained from the analysis of the LSS imaging data and using standard morphometry of the stained monolayer are shown in Fig. 5 (b) and (c) respectively. The agreement between the spatial distributions of nuclear size in these two images is evident. As can be seen, the nuclei are smaller (average size $d \approx 13$ μm) in the right field and tend to be larger in the remaining regions (some of these nuclei are as large as 15 μm).

3. MEASUREMENT OF CONCENTRATION OF NUCLEAR CHROMATIN WITH LSS IMAGING

As can be seen, LSS imaging can elucidate subtle morphological variations such as a difference in nuclear sizes of a fraction of a micron. Furthermore, the analysis allows determination of the refractive index of the nuclei relative to the surrounding cytoplasm. The refractive index of nuclei and many other cell organelles is a linear function of the ratio of the solid mass of an organelle, which is formed by DNA, RNA, and proteins, to its volume.[15-17] A higher concentration of nuclear chromatin (the solid component of the nucleus) results in a deeper staining of these nuclei with nuclear stains, such as H&E. This effect is referred to as hyperchromasia and has been known to correlate with dysplasia and malignancy.[9,18]

To determine the concentration of nuclear chromatin using LSS one needs to estimate so-called

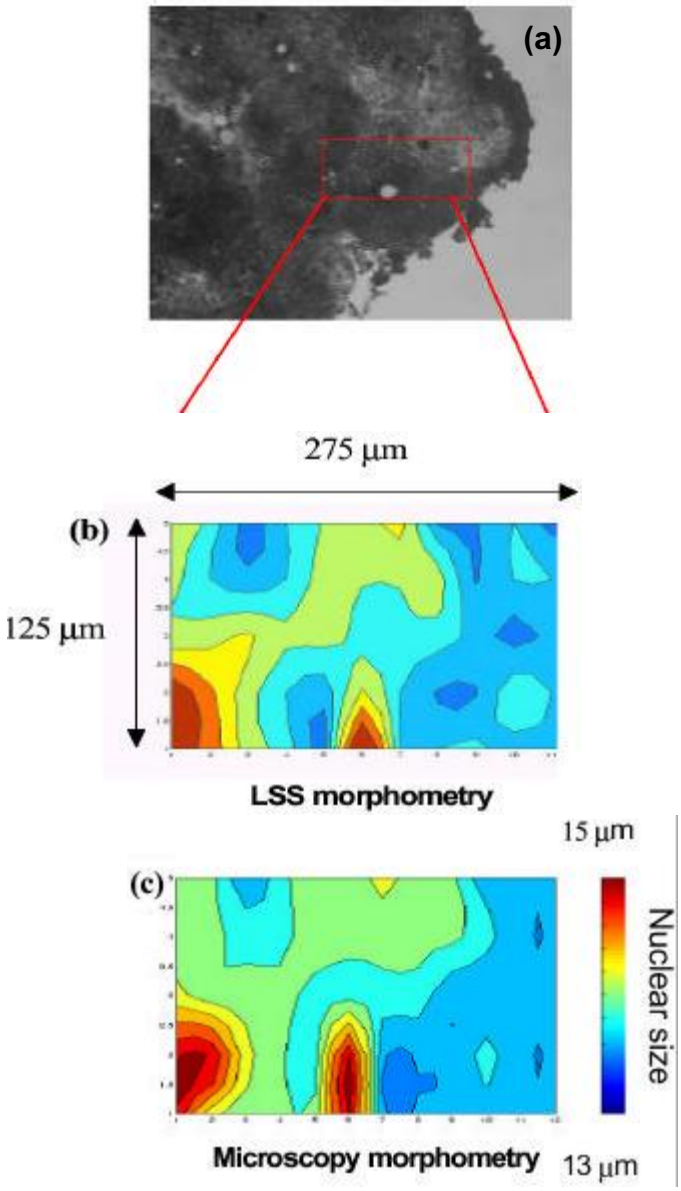

Figure 5. LSS imaging of a cell monolayer. See text for details.

mass ratio η using the following equation[24]

$$n_n = n_0 + \alpha\eta \ , \tag{2}$$

where n_n is the refractive index of the nucleus measured using LSS, n_0 is the refractive index of water, α is a proportionality coefficient, which was found to be equal 0.18 for most cellular structures including the cell nucleus, major organelles and the cytoplasm, and $\eta = \dfrac{\rho_n}{\rho_0}$ with ρ_n the mass density of the chromatin measured in mass/volume-units and ρ_0 the mass density of water.

According to equation (2), the refractive index of a nucleus equals to that of water when the concentration of chromatin is zero and approaches approximately 1.514 when the nucleus is almost completely filled with proteins, DNA, and RNA. Thus, chromatin density ρ_n can be found as

$$\rho_n = \frac{\rho_0}{\alpha}\left(n_n - n_0\right). \tag{3}$$

The standard error of such measurements can be estimated as

$$\frac{\delta\rho_n}{\rho_n} = \frac{\alpha\eta_c n}{n_n - n_0}\sqrt{\left(\frac{\delta\eta_c}{\eta_c}\right)^2 + \left(\frac{\delta n}{n}\right)^2} \ , \tag{4}$$

where δ denotes a standard error of measurement. Substituting $\dfrac{\delta\eta_c}{\eta_c} \approx 0.2$ and $\dfrac{\delta n}{n} \approx 0.2$. into (4) we obtain $\dfrac{\delta\rho_n}{\rho_n} \approx 0.05$. According to LSS studies with cell monolayers, *ex vivo* and *in vivo* tissues, most epithelial cell nuclei have $\rho_n \sim 0.3 - 0.6$ pg/μm^3 and, therefore, $\delta\rho_n \sim 0.015 - 0.03$ pg/μm^3.

Not only does LSS enable assessment of the concentration of nuclear chromatin or other cellular organelles, but it allows obtaining information about the total or dry mass of the organelle, i.e. cell nucleus. Nuclear chromatin mass was shown to correlate with the amount of chromosomal DNA present in the nucleus.[16,19] Increased amount of DNA is thought to be an indicator of increased DNA transcription and protein synthesis associated with higher proliferative activity of precancerous and cancerous cells.[20] Currently, the amount of DNA can be measured using ploidy analysis on cells removed from the body. There is no technique that would allow such analysis to be performed *in vivo* or even *in vitro* on living cells. Moreover, ploidy analysis does not provide objective quantitative information so that the amount of DNA from one tissue sample could not be compared with that of another.

For a nucleus of volume V, the chromatin mass can be found as $M_n = V\rho_n$. Although LSS allows measurement of nuclear diameter d, the volume cannot simply be expressed in terms of d unless certain assumptions about the shape of the nucleus are made. Typical nuclei have shape that resembles sphereoids and are randomly oriented in tissue. Therefore, it is reasonable to estimate nuclear volume as that of a sphere with diameter d, $V \approx \dfrac{4}{3}\pi\left(\dfrac{d}{2}\right)^3$. Thus, the dry mass of nuclear chromatin can be approximated as

$$M_n \approx \frac{4}{3}\left(\frac{d}{2}\right)^3 \frac{\pi\rho_0}{\alpha}\left(n_n - n_0\right). \tag{5}$$

Determination of chromatin mass using (5) is by no means rigorous. However, it can provide some information about how much chromatin a *population* of cell nuclei contains on average. In fact, as shown Paramonov[21], equation (5)

is relatively accurate, $\frac{\delta V}{V} \leq 0.1$, in estimating the average volume of a population of randomly oriented spheroids with shape parameter, which is defined as the ratio of the longer dimension of the spheroid to its smaller dimension, not exceeding 2. Epithelial nuclei typically fall into this category: their shape parameter rarely exceeds 2 and they are randomly oriented. Even when there exists certain preferred orientation of the nuclei in respect to the basement membrane, in many cases the nuclei are randomly oriented in respect to an externally defined direction, such as the direction of the propagation of the incident light, due to the folding of the epithelial basal surface.

4. *IN SITU* LSS IMAGING

In order to test the applicability of LSS imaging we performed experiments with *ex vivo* colon tissue samples that were obtained immediately after resection from patients undergoing colectomy for familial adenomatous polyposis. Colonic adenomas are precancerous dysplastic lesions exhibiting all of the characteristics of dysplastic lesions, including cell nuclear enlargement, pleomorphism, and hyperchromasia. The adenomas are surrounded by normal tissue covered by a single layer of epithelial cells. Images of an adenoma surrounded by nondysplastic colon mucosa were obtained using the LSS apparatus. For each pixel (25 μm x 25 μm) of the imaged field (1.3 cm x 1.3 cm) a spectrum of light backscattered by the nuclei was first distinguished from the rest of the reflected light using polarization discrimination and then analyzed using the Mie theory-based computerized algorithm. The parameters obtained were the size and refractive index of the nuclei in each pixel. The imaged field was divided into 125 μm x 125 μm regions and the percentage of nuclei larger than 10 μm was obtained for each of these areas. Previous studies[11] have shown that this statistic, which characterizes the degree of nuclear enlargement, is highly significant for diagnosis of dysplastic lesions in the colon and several other organs.

The resulting color-coded plot is shown in Figure 6(a). As expected, the nuclei are enlarged in the central, adenomatous region, but not in the surrounding non-dysplastic tissue. Figure 6(b) is an LSS image of the spatial distribution of the mass of nuclear chromatin displayed in units of picograms per nucleus. These values were derived from the knowledge of the diameter and the refractive index of the nuclei, obtained from our LSS image. One can see that in the region of the polyp, the chromatin content is larger than in the surrounding normal tissue. This condition is an indication of dysplasia.

In contrast to conventional images of cells or tissues, the LSS-based imaging provides quantitative images of the parameters characterizing certain histological properties, such as cell nuclear enlargement, pleomorphism and increased chromatin content. Methods for providing such quantitative information without tissue removal are not currently available. It is important to emphasize that in contrast to conventional optical images, the images produced by light scattering spectroscopy do not depict tissue structure as a microphotograph would. Rather, they provide quantitative maps of distributions of parameters such as nuclear enlargement, degree of pleomorphism, and increased chromatin content, features that relate to the functional state of the tissue. Furthermore, pixel size and the wavelength of light do not limit the resolution of the technique. For example, in our tissue images the nuclear size is determined with an accuracy exceeding 0.1 μm, whereas the pixel size is 25 μm and the light wavelength ~ 0.5 μm. Such accuracy is

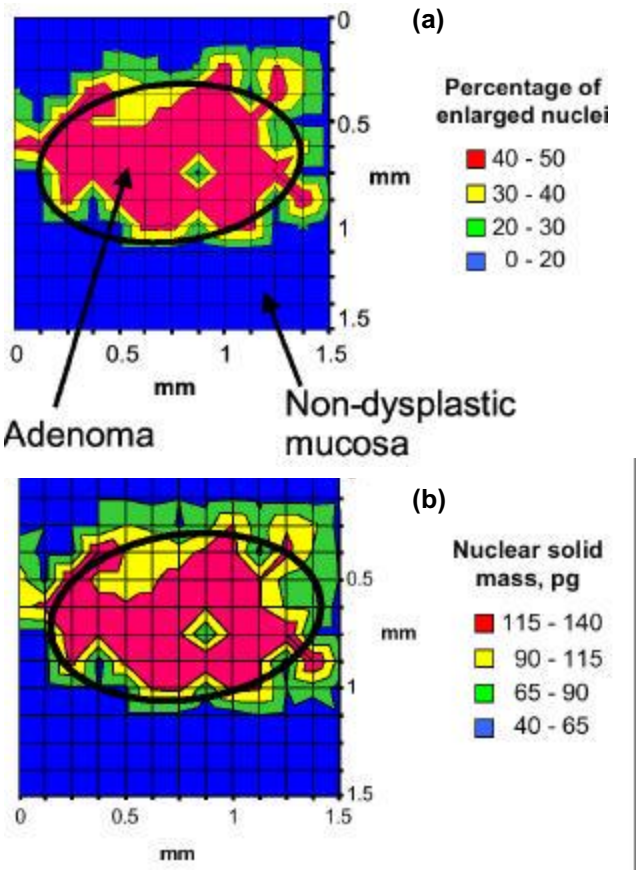

Figure 6. LSS imaging of colon adenoma. See text for details.

obtainable because the information is derived from spectral variations of the backscattered light, an interference phenomenon sensitive to very small changes in the cell nuclear parameters. LSS makes it possible to observe these variations, and measuring them enables the nuclear size and refractive index to be determined. The results reported here indicate the promise of LSS-based imaging for clinical use, as well as for a biomedical research tool to study the dynamics of nuclear changes accompanying the progression of cancer and other diseases. Particularly important applications include detection of early cancer and precancerous conditions in cervix and oral cavity.

5. MEASUREMENT OF SUBCELLULAR STRUCTURE AT SUBMICRON SCALES WITH A/LSS

The capabilities of LSS are not limited to measuring cell nuclear size and chromatin content. The technique can also provide quantitative information about internal structure of the nuclei as well as other subcellular structures. It is known that large particles, such as nuclei, scatter predominantly in the forward and near backward directions and, for such angles, cell nuclei are major sources of scattering. On the other hand, light scattered by structures smaller than the wavelength of light dominates the scattering signal at larger backscattering (smaller scattering) angles. Thus, analysis of the spectra of light backscattered at larger angles can reveal information about sub-nuclear inclusions and subcellular organization at submicron scale.

A novel modality of LSS, scattering angle sensitive LSS (a/LSS), enables measurement of both the spectral and angular distributions of scattered light[12]. In a/LSS, the angular distribution of scattered light is imaged onto the CCD by exploiting the Fourier transform properties of a lens. A schematic diagram of the apparatus is shown in Fig. 7. A beam from a broad-band xenon arc lamp (Oriel, Inc.) is spatially filtered and collimated by lenses L1 (f = 170 mm), L2 (f = 95 mm), and the aperture A1. A series of narrow-band optical filters F (Edmund Scientific, FWHM = 20 nm) with center wavelengths λ_i, selects a narrow wavelength band. In our experiments λ_i= 532, 550, 568, 589, 620, 650, 671, 694 nm. The beam is then polarized by polarizer P1, passed through a second aperture A2 which is used to reduce the diameter of the beam to about 3 mm, reflected from the mirror M, and made incident on the sample stage, on which the sample is mounted. The mirror M is set such that the beam strikes the sample stage at an angle of about 15 degrees, which prevents the specular reflection from being imaged. The sample stage is placed at one focal plane FP1 of lens L3 (f = 125 mm), while a 512 x 512 pixel, 16 bit cooled CCD camera (Princeton Instruments, 512TK) is placed at the other focal plane FP2, where a two dimensional map of the angular distribution of the backscattered light is formed. The polarization state of the scattered light to be viewed is selected by the analyzer P2.

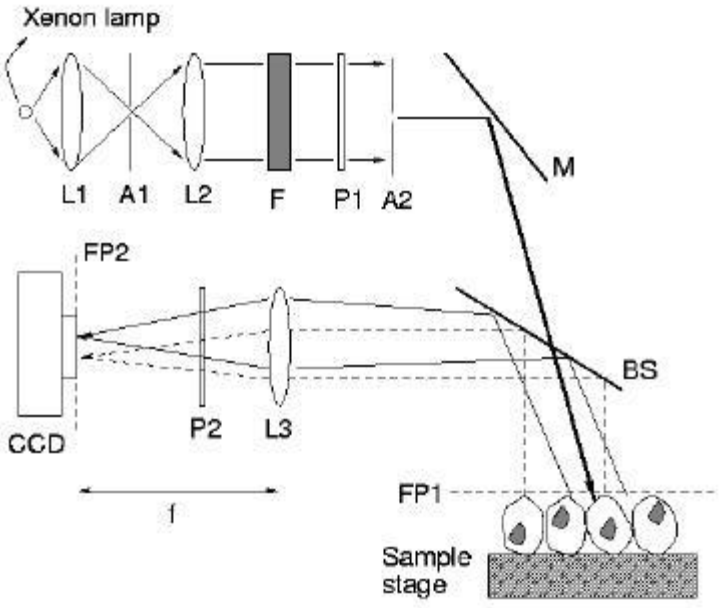

Figure 7. A/LSS apparatus. L1, L2: collimating lenses; A1, A2: Iris diaphragms; F: narrowband filter; P1, P2: polarizers; M: Mirror, BS: 50:50 beam splitter, CCD: 16 bit CCD camera. The sample is mounted on the sample stage.

The a/LSS device has been calibrated in experiments with polystyrene beads and cell monolayers. The results show that the cell nuclei scatter predominantly within a narrow cone (1-2^o) near the exact backward direction, in agreement with previous results as well as theoretical calculations. Thus, the signal measured within a sufficiently

narrow solid angle provides information about the size and refractive index of the cell nuclei. However, the signal scattered into larger scattering angles (>3°), particularly with 45° azimuth in respect to the polarization of the incident light, provides information about sub-cellular structure at the sub-micron scale. The latter angular range was used in experiments with monolayers of benign mesothelial intestinal cells and T84 tumor colonic cells, to measure the size distribution of sub-micron structures within the cells and their nuclei.

In these experiments, the LSS signals could not be fitted under the assumption that the particles are normally distributed for any given mean size from 0.3 to 15 μm. Moreover, other types of size distributions, such as top-hat, exponential, or skewed-normal could not fit the data either. The spectra were found to be best fitted only when an inverse power-law distribution for the number of particles was used, where the concentration $N(d)$ of particles with a diameter d, is given by $N(d) \propto d^{-\beta}$, with size exponent β not dependent on d and characterizing the variations of refractive index inside the cells and, thus, the variations of intracellular density. To obtain the values of β, Mie-theory based inversion procedure was used to fit the data as discussed above. The sizes were assumed to be distributed between 0.01 and 1.5 μm according to a power-law, with fitting parameter β. For T84 tumor cells, we found β to be approximately 2.2, whereas for normal mesothelial cells the best fit was obtained for β = 2.7. Thus, the size distribution of the T84 colon tumor cells is shifted with respect to that of the normal cells, with an increase in the relative number of large intra-cellular and intra-nuclear structures.

The smaller values of the size exponent for malignant cells can be correlated with certain alterations of normal cell structure associated with cancerous changes. For example, a smaller value of β in the size distribution of the intra-nuclear structure correlates with the visual perception of clumped and rough chromatin when a stained tissue sample is microscopically evaluated. Pathologists evaluating H&E-stained samples of precancerous cells frequently observe such changes.

Smaller values of β for malignant cells may also indicate higher structural entropy. The entropy of a 3D structure can be defined as

$$S = \sum_j N_j \ln \frac{1}{N_j} , \tag{6}$$

where N_j is the number (population) density of structural species of type j. This entropy characterizes the degree of internal disorganization of the structure. According to this definition, if there is only one species present, then N_1=1 and S=0. When the structural species are distributed in size almost continuously according to the power-law with spectral exponent β, the entropy can be approximated as follows

$$S \approx \int N(d') \ln \frac{1}{N(d')} dd' \propto \frac{\beta}{(\beta - 1)}. \tag{7}$$

Expression (7) indicates that the entropy increases monotonously when β decreases and approaches 1. Therefore, smaller values of β for dysplastic and malignant nuclei may indicate higher entropy and, thus, higher disorganization of the cell structure.

Finally, a difference in β may be related to change in the fractal properties of the malignant cells. It can be shown that β relates to the fractal dimension $d_f^{(p)}$ of the planar (2D) images of the cells and some large subcellular structures such as the nucleus as follows, $d_f^{(p)} \approx \beta$. Moreover, the fractal dimension $d_f^{(m)}$ of a 3D fractal formed by spatially distributed internal components with $N(d) \propto d^{-\beta}$ is related to β as well. Therefore, the change in β for precancerous and cancerous cells and tissues indicates the change of both $d_f^{(p)}$ and $d_f^{(m)}$, which, in turn, may indicate the loss of structural complexity of the cells[22,23]. Moreover, objects with smaller $d_f^{(p)}$ typically appear with coarse, clumped structure of their components. For example, if $d_f^{(p)}$ of a cell nucleus is decreased, such nucleus would be perceived by a pathologist examining a stained histology slide as one exhibiting some of the characteristic histological markers of precancer and malignancy related to the altered chromatin texture, namely chromatin clumping, coarse texture and prominent margination of chromatin. Further studies are needed to elucidate the histological correlate of this observation as well as its functional implications.

ACKNOWLEDGEMENTS

This work was supported by NIH grant P41-RR02594, NIH grant R01-CA53717, and CIMIT grant 731-3489-5. The T84 cells were generously provided by Dr. Wayne Lencer, Children's Hospital, Boston, Massachusetts.

REFERENCES

1. J.R. Mourant *et al.* "Spectroscopic diagnosis of bladder cancer with elastic light scattering". *Laser Surg. Med*. **17**, 350-357 (1995).
2. L.T. Perelman, V. Backman, M. Wallace, G. Zonios, R. Manoharan,, A. Nusrat, S. Shields, M. Seiler, C. Lima, T. Hamano, I.Itzkan, J.Van Dam, J.M. Crawford, M.S. Feld, "Observation of periodic fine structure in reflectance from biological tissue: A new technique for measuring nuclear size distribution". *Phys. Rev. Lett.* **80**, 627-630 (1998).
3. R. Drezek, A. Dunn, R. Richards-Kortum, "Light scattering from cells: finite-difference time-domain simulations and goniometric measurements," *Applied Optics* 38, 3651-3661 (1999).
4. J.R.Mourant, M.Canpolat, C.Brocker, O.Esponda-Ramos, T.M.Johnson, A. Matanock, K. Stetter, J.P. Freyer, "Light scattering from cells: the contribution of the nucleus", *J. Biomed. Optics* **5**, 131-137 (2000).
5. J.R. Mournat, T.M. Johnson, and J.P. Freyer, "Characterizing mammalian cells and cell phantoms by polarized backscattering fiber-optic measurements," *Applied Optics* **40**, 5114-5123 (2001).
6. J.R. Mourant, T. Fuselier, J. Boyer, T. M. Johnson, and I.J. Bigio, "Predictions and measurements of scattering and absorption over broad wavelength ranges in tissue phantoms," *Applied Optics* **36**, 949-957 (1997).
7. R. Drezek, A. Dunn, R. Richards-Kortum,"A pulsed finite-difference time-domain (FDTD) method for calculating light scattering from biological cells over broad wavelength ranges," *Optics Express* **6**, 147-157 (2000).
8. A. G. Yodh and B. Chance, "Spectroscopy and imaging with diffusing light," *Phys. Today* **48**, No. 3, 34 (1995).
9. R. S. Cotran, S. L. Robbins, and V. Kumar, *Robbins Pathological Basis of Disease* (Saunders, Philadelphia, 1999).
10. V. Backman, R. Gurjar, K. Badizadegan, I. Itzkan, R. R. Dasari, L. T. Perelman, and M. S. Feld, "Polarized light scattering spectroscopy for quantitative measurement of epithelial cellular structures in situ", *IEEE J. Sel. Top. Quantum Electron*., **5**, 1019-1026, (1999).
11. V. Backman, M.B. Wallace, L.T. Perelman, J.T. Arendt, R. Gurjar, M.G. Muller, Q. Zhang, G. Zonios, E. Kline, T. McGillican, S. Shapshay, T. Valdez, J. Van Dam, K. Badizadegan, J.M. Crawford, M. Fitzmaurice, S. Kabani, H.S. Levin, M. Seiler, R.R. Dasari, I. Itzkan and M.S. Feld, "Detection of preinvasive cancer cells *in situ"*. *Nature*, **406**, 35 (2000).
12. V. Backman, V. Gopal, M. Kalashnikov, K. Badizadegan, R. Gurjar, A. Wax, I. Georgakoudi, M. Mueller, C.W. Boone, R.R. Dasari, and M.S. Feld, "Measuring Cellular Structure at Submicron Scale with Light Scattering Spectroscopy", *IEEE J. Sel. Top. Quant. Elect.*, December 2001.
13. R. Gurjar, V. Backman, K. Badizadegan, R. Dasari, I. Itzkan, L.T. Perelman, and M.S. Feld, "Imaging of Human Epithelial Properties with Polarized Light Scattering Spectroscopy", *Nature Medicine*, **7**, 1245-1248 (2001).
14. J.C. Russ, *The Image Processing Handbook* (CRC Press, Boca Raton, Ann Arbor, London, Tokyo, 1992).
15. H.C. Davies, E.M. Deeley, E.F. Denby, "Attempts at measurement of lipid, nucleic acid and protein content of cell nuclei by microscope-interferometry". *Exp. Cell Res*., Suppl. 4, 136-149 (1957).
16. H.G. Davies, *General Cytochemical Methods* (Danielli, J.F., ed.) Vol I. (Academic Press, New York, 1958).
17. L. Lee, A. J. Pappelis, G.A. Pappelis, H.M. Kaplan, "Cellular and nuclear dry mass and area changes during human oral mucosa cell development". *Acta Cytol*. **17**, 214-219 (1973).
18. C.W. Boone *et al. "*Quantitative grading of rat esophageal carcinogenesis using computer-assisted image tile analysis". *Cancer Epidemiology, Biomarkers & Prevention,* **9**, 495-500 (2000).
19. G.L. Brown, McEwan, M., Pratt, M. *Nature*, **176**, 161-162 (1955).
20. J.V. Watson, *Introduction to Flow Cytometry* (Cambridge University Press, Cambridge, 1991).
21. L.E. Paramonov, "On optical equivalence of randomly oriented ellipsoidal and polydisperse spherical particles", *Opt. Spekt*., **77**, 660-663 (1994).
22. Mandelbrot, *Fractal Geometry of Nature* (Freeman & Co, 1988).
23. A.J. Einstein, Wu HS and Gil J, "Self-Affinity and Lacunarity of Chromatin Texture in Benign and Malignant Breast Epithelial Cell Nuclei", **80**, 397-400 (1998).
24. J.M. Schmitt and G. Kumar, "Optical scattering properties of soft tissue: a discrete particle model". *Appl. Opt*., **37**, 2788-2797 (1998).